A first-principles model of birefringent porous silicon

Yuri Bonder and Chumin Wang[a)]
Instituto de Investigaciones en Materiales, Universidad Nacional Autónoma de México, Apartado Postal 70-360, 04510 Mexico Distrito Federal, Mexico

(Received 28 December 2005; accepted 13 June 2006; published online 29 August 2006)

Optical properties of birefringent porous silicon (*b*-PSi) layers are studied by means of the density functional theory (DFT) within the local density approximation (LDA). A systematic study of crystalline silicon (*c*-Si) is performed in order to validate this DFT-LDA calculation of optical properties of semiconductors. In order to simulate *b*-PSi, elliptical columns of 1–4 atoms are removed from a *c*-Si supercell of 16 atoms in the [100] and [010] directions. The dangling bonds are saturated with hydrogen atoms. A geometry optimization is carried out to get the minimum energy configuration. The results of the refractive index (n) show an enhanced anisotropy and the difference $\Delta n = n_{[1\bar{1}0]} - n_{[001]}$ agrees well with experimental data. In particular, measurements in p^+ and p^{++} doped *b*-PSi samples are consistent with the results obtained in the limit cases of pore branches along the [001] direction and the perfectly straight pores, respectively. © *2006 American Institute of Physics*. [DOI: 10.1063/1.2335669]

I. INTRODUCTION

Materials built from nanoclusters have exceptional properties such as improved hardness, increased ductility, interesting magnetic, and optoelectronic properties.[1] In consequence, these nanostructured materials could be used in a wide range of industrial, biomedical, and electronic applications. The origin of their peculiar behaviors is thought to be related to the quantum confinement and the large percentage of atoms at interfaces.[2]

Microelectronics is perhaps the most important technological achievement in the past century because it has modified the lifestyle of billions of people. Nowadays, this technology is almost exclusively based on silicon, since it is the second most common element on the earth's crust and a material over which SiO_2 insulating layers are easily grown on.[3] However, crystalline silicon (*c*-Si) has an indirect band gap of 1.1 eV which limits its application in optoelectronics. The search for an active optical semiconductor in the visible light range, compatible with current microelectronic technology, took a big step forward when in 1990 the efficient photo- and electroluminescences of porous silicon (PSi) at room temperature were discovered.[4]

Porous silicon has a spongelike structure basically formed by interconnected *c*-Si clusters and wires at nanometric scale. This structure can be obtained from electrochemical etching of *c*-Si in hydrofluoric acid solutions;[4] a process which is particularly simple, cheap, and suitable to be integrated into the fabrication of microchips. Consequently, PSi is expected to serve a wide variety of uses, for example, as a sensitive gas sensor,[5] a tunable photonic material,[6] a visible light-emitting device integrated into microelectronic circuits,[7] and as an efficient interface between biological and electronic systems.[8]

It is well known that there is a preferential growth of pores along the equivalent [100] crystallographic directions in *c*-Si for all doping concentration and anodization conditions.[9,10] Hence, a birefringent PSi (*b*-PSi) sample can be obtained by etching (110)-oriented *c*-Si wafers, in which the pores lie on (001) planes. This particular morphology causes a strong dielectric anisotropy for normally incident light polarized in the $[1\bar{1}0]$ and [001] directions.[11] This property could be used to produce sensors able to analyze the adsorption of atoms and molecules in negligible quantities.[12] In addition, its multilayer arrangements could serve as a dichroic microcavity with its transmission dependent on the polarization direction of the incident light.[11]

Recent experiments have shown that there is a qualitative difference in the optical anisotropy response for *b*-PSi samples obtained from p^+ and p^{++} *c*-Si wafers.[13] Indeed, a sign change is found in $\Delta n = n_{[1\bar{1}0]} - n_{[001]}$, where $n_{[1\bar{1}0]}$ and $n_{[001]}$, respectively, represent the refractive index for light polarized along the $[1\bar{1}0]$ and [001] directions. Moreover, this change of sign is combined with a significant increase of $|\Delta n|$ for p^{++} samples. The goal of this investigation is to understand the main structural factors that cause the optical anisotropy of *b*-PSi. For this purpose we have performed a first-principle study of *b*-PSi based on a supercell model. The numerical calculations are carried out within the density functional theory (DFT). In order to verify the method, a systematic analysis has been done for the zero-porosity limit case, corresponding to *c*-Si, and the obtained results are compared with experimental data.

II. CALCULATION METHOD

The properties of a material can be studied empirically, semiempirically, or through a first-principles model. The DFT is undoubtedly the most popular first-principles method to study ground-state properties of semiconductors when the electrons are weakly correlated. This theory is based on the fact that the correct ground-state electronic density can be obtained by self-consistently minimizing the total energy

[a)]Author to whom correspondence should be addressed; FAX: +52 55 5616 1251; electronic mail: chumin@servidor.unam.mx

density functional.[14] In addition, the Born-Oppenheimer adiabatic approximation is assumed in order to decouple the motion of nuclei and electrons.

In DFT the exchange-correlation energy functional can be calculated by using the local density approximation (LDA), which assumes that the system locally behaves like a homogeneous electron gas with the same density as the real one. In particular, the correlation energy is obtained with the Perdew-Zunger method which leads to exact Monte Carlo results in the high and low density limits and it is considered the most precise LDA method to calculate this energy.[15] Unfortunately, for semiconductors and insulators the LDA underestimates the band gap by 30%–50%.[16] This discrepancy can be overcome by introducing the many-body *GW* approximation: the first term in an expansion of the self-energy operator in terms of the dressed Green's function (G) and the dynamically screened Coulomb interaction (W).[17] It has been numerically demonstrated that the *GW* spectrum can be reproduced by rigidly shifting the LDA conductions bands to higher energies through a scissors operator (ΔE),[18] which provides a simple manner to calculate optical properties of semiconductors. Moreover, the LDA gives the correct sum rule for the exchange-correlation hole, leading to properly calculated optical properties.[19]

All the calculations in this article are done with the CASTEP codes developed at Cambridge University[20] which are considered to be one of the most precise DFT plane-wave pseudopotential programs. Specifically, the electronic wave functions are expanded in a plane-wave basis set truncated at a certain cutoff energy (E_c). To properly calculate optical properties, norm-conserving pseudopotencials are used in which the scattering process is correctly reproduced by requiring the integrals of squared amplitudes of pseudo- and all-electron wave functions to be identical inside the core region.[16] The first Brillouin zone is represented by a **k**-point sampling with a constant spacing Δk, where each point has a specific weight given by the Monkhorst and Pack method.[21]

In addition, full geometry optimizations are performed, leading the atoms to their minimal energy positions, by means of the Broyden-Fletcher-Goldfarb-Shanno (BFGS) quasi-Newton minimization algorithm[22] in the configuration space. Then, through Fermi's golden rule, the imaginary part of the dielectric function (ε) can be written as[23]

$$\mathrm{Im}[\varepsilon(\omega)] = \frac{2e^2\pi}{\Omega\varepsilon_0}\sum_{k,v,c} |\langle\Psi_k^c|\hat{\boldsymbol{e}}\cdot\boldsymbol{r}|\Psi_k^v\rangle|^2\delta(E_k^c - E_k^v - \hbar\omega), \tag{1}$$

where $\hat{\boldsymbol{e}}$ is the light-polarization unitary vector, Ω is the volume of the supercell, E_k^v and E_k^c are the energies corresponding to the wave functions Ψ_k^v and Ψ_k^c, respectively. Notice that the superscript indices v and c stand for valence and conduction bands, respectively. The real part of the dielectric function is linked to Im[ε] by the Kramers-Kronig transformation. For nonmagnetic materials, the complex refractive index, $N=n+in_c$, can be calculated through $\mathrm{Re}[\varepsilon]=n^2-n_c^2$ and $\mathrm{Im}[\varepsilon]=2nn_c$. It is worth mentioning that a smearing width (η), specifying the Gaussian broadening of the dielectric function, is introduced to include thermal, structural, and/or chemical impurity effects, all presented in real samples and measurement conditions.

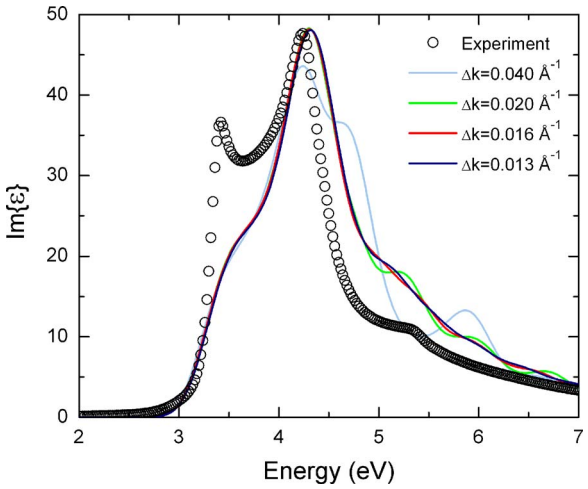

FIG. 1. (Color online) The imaginary part of the dielectric function (Im[ε]) vs the photon energy for c-Si with different **k**-point spacing Δk (solid lines) in comparison with experimental data (open circles).

III. VALIDATION OF THE METHOD

In general, first-principle calculations can be divided in two main parts: geometry optimization and calculation of physical properties. For this investigation, calculations of optical properties are carried out at the ultrafine precision level provided by CASTEP within the MATERIALS STUDIO framework. The same number of valence and conduction bands is always considered in order to ensure the optical response up to 7 eV. The choice of improved values of E_c, Δk, ΔE, and η has been verified by comparing the obtained results with those of c-Si. In particular, it is known that E_c should be large due to the presence of hydrogen atoms and it is set at 900 eV which is the minimum value so that the optical spectra of silane molecules are essentially unchanged. On the other hand, Δk, ΔE, and η are chosen in comparison with experimental data of Im[ε] from c-Si.[24] In Fig. 1 the calculated Im[ε] of c-Si is shown for different Δk and fixed E_c =900 eV, ΔE=0.6 eV, and η=0.18 eV. Notice that theoretical results reproduce the general behavior of the experimental Im[ε], except for the peak at 3.42 eV. This discrepancy is found even when the *GW* approach[17] or other methods beyond LDA are employed.[25]

In Fig. 1, it can be observed that the high-energy behavior of Im[ε] is sensitive to the number of **k** points taken to evaluate Eq. (1), but no significant modifications are exhibited for $\Delta k < 0.016$ Å^{-1}. In consequence, the Δk used in all the b-PSi optical property calculations is set at 0.016 Å^{-1}. Similar analyses as the aforementioned have been done for other parameters, including those in the geometry optimization calculations. The final values for all the parameters used in the rest of this article are summarized in Table I. In particular, this set of parameters is used to calculate Δn of c-Si obtaining 2.01×10^{-5} at a wavelength λ=1150 nm, close to the experimental data of 5.04×10^{-6}.[26] This aniso-

TABLE I. Summary of the parameters used in the calculations of *b*-PSi.

Physical quantity	Geometry optimization	Optical properties
Total energy convergence tolerance	2.0×10^{-5} eV/at.	
Maximum force convergence tolerance	0.05 eV/Å	
Maximum stress convergence tolerance	0.1 GPa	
Maximum displacement convergence tolerance	0.002 Å	
Self-consistent field tolerance	5×10^{-7} eV/at.	5×10^{-7} eV/at.
Energy cutoff (E_c)	900 eV	900 eV
k-point sample spacing (Δk)	0.04 $Å^{-1}$	0.016 $Å^{-1}$
Scissors operator (ΔE)		0.6 eV
Smearing width (η)		0.18 eV
Number of conduction bands		The same number of valence bands

tropic dielectric response in cubic crystals could be caused by the symmetry breaking of the finite Δk involved in optical transitions.

IV. MODELING *B*-PSI

A supercell of 16 atoms can be built by adding in the z direction two cubic *c*-Si cells formed by eight atoms. In *b*-PSi the pores are oriented in the [100] and [010] crystalline directions, which can be produced in several ways. For example, two separated Si atoms (larger spheres) are removed as shown from its (x) and (y) views in the inset of Fig. 2(a), where all the dangling bonds are saturated with hydrogen atoms (smaller spheres). Notice that this supercell has identical pores in all the equivalent [100] directions. If the porosity is defined as the ratio of the removed Si atoms over the total number of Si atoms in the original supercell, the supercell in Fig. 2(a) has a porosity of 12.5%. Other possible ways to excavate *b*-PSi pores are presented in the insets of Figs. 2(b) and 2(c) from the x and y views, having porosities of 6.25% and 12.5%, respectively. It is worth mentioning that these two supercells have no pores in the [001] direction, and that all the supercells of Fig. 2 are structures obtained from geometry optimization processes.

Starting from the geometrically optimized supercells, the calculation of electronic band structures is performed. The results exhibit an almost direct band gap wider than the one of *c*-Si, as in Ref. 27. The real part of the refractive index (n) is calculated for [110] incident light polarized along different directions with a fixed wavelength $\lambda=514$ nm. The results are shown in Fig. 2 for the *b*-PSi structures illustrated in the corresponding insets, where the 0° and 90° stand, respectively, for the $[1\bar{1}0]$ and [001] polarization directions. Observe that the polarization independence of n in Fig. 2(a) is caused by the pore's cubic isotropy, which corresponds to the limit case that the pores grow equally in all the preferential directions. Another possible *b*-PSi structure is analyzed in Fig. 2(b), where the pores completely lie on (001) planes leading to $\Delta n=0.02$, much larger than the value of 2.24×10^{-5} for *c*-Si at the same wavelength. In Fig. 2(c), the

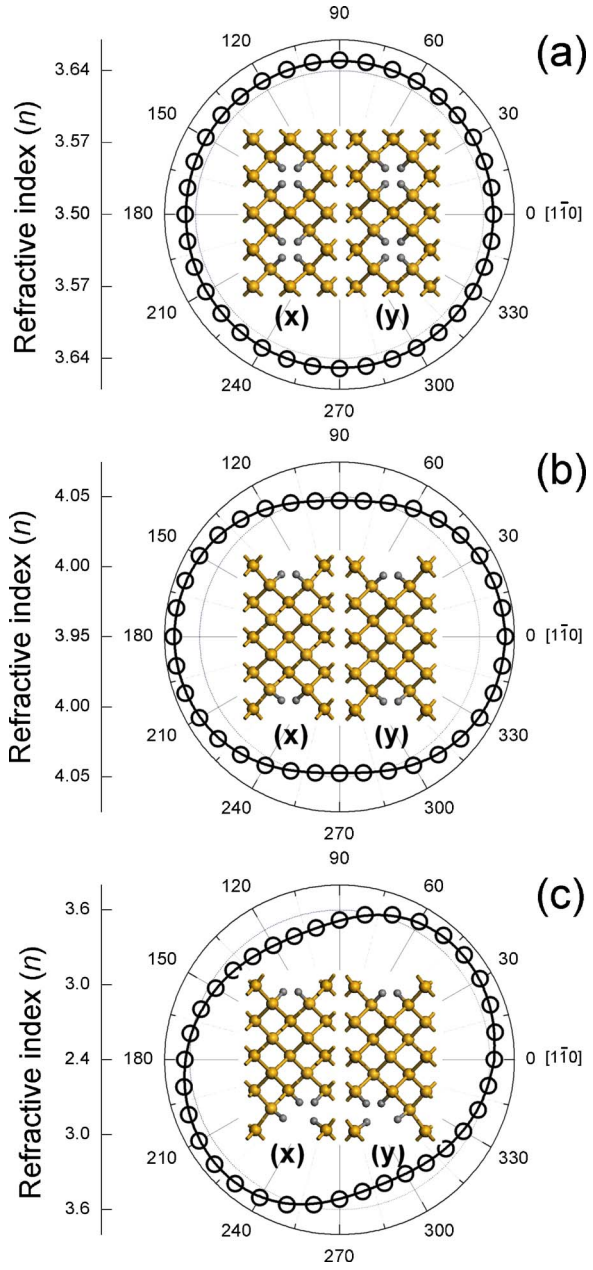

FIG. 2. (Color online) The real part of the refractive index (open circles) vs the light polarization angle for *b*-PSi built by removing (a) two separated Si atoms (larger spheres in insets), (b) one Si atom, and (c) two nearest-neighbor Si atoms, from an initial *c*-Si supercell of 16 atoms. All the dangling bonds are saturated with hydrogen atoms (smaller spheres in insets). The corresponding structures are shown in the insets from its x and y views.

maximum value of n is rotated by about 30° towards the [001] direction with respect to Fig. 2(b). This fact arises from the elliptic morphology of the pore, which has a small extension along the [001] direction. Moreover, the pores of Figs. 2(a) and 2(b) represent, respectively, those found in *b*-PSi samples with low and high *p*-type doping concentration, since the pores grow almost exclusively along the [100] and [010] directions in high doped (110)-oriented *c*-Si wafers.[13]

In order to study *b*-PSi with larger porosities, two additional supercells similar to those presented in the insets of Figs. 2(b) and 2(c) are constructed by removing elliptical columns of three and four nearest-neighbor Si atoms, obtaining *b*-PSi with 18.75% and 25.0% porosities, respectively. It

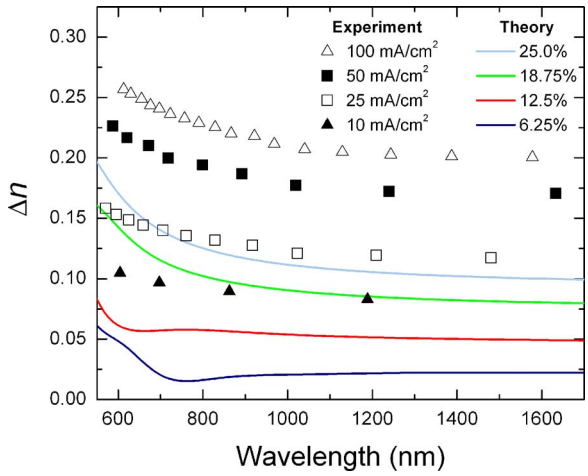

FIG. 3. (Color online) Calculated optical anisotropy of the refractive index ($\Delta n = n_{[1\bar{1}0]} - n_{[001]}$) as a function of the light wavelength for four *b*-PSi structures with porosities specified in the figure, together with experimental data obtained from p^{++} doped *b*-PSi samples.

is worth mentioning that four Si atoms are the maximum number of atoms that can be removed from a 16 atom supercell in order to avoid both, the formation of pores in [001] direction and the fragmentation of the solid. In Fig. 3 the anisotropy of the refractive index (Δn) is illustrated as a function of the light wavelength for the previously discussed *b*-PSi supercells, next to the experimental data obtained from highly doped *b*-PSi samples.[13] It is well known that etching *c*-Si wafers with higher electric current densities generates PSi samples with larger porosities.[28] It can be observed in Fig. 3 that Δn decreases when the wavelength increases and grows with porosity, in the same way as the experimental data. This fact can be understood as follows: if the photon energy is much smaller than the optical gap, it can be proved using the Kramers-Kronig relations[29] that n always decreases as the wavelength grows, independently of the light polarization. Hence, for the spectral region of Fig. 3, Δn is proportional to n and decays as the wavelength increases. This proportionality has been numerically verified.

V. CONCLUSIONS

We have performed a first-principles calculation of *b*-PSi through small supercells, which are able to retain the main physical features of real *b*-PSi samples. The parameters used in this calculation have been systematically explored and validated for the limiting case of *c*-Si. In particular, the extremely small optical anisotropy in the refractive index (Δn) of *c*-Si can be reproduced in comparison with experimental data and the analytical prediction of Lorentz,[30] which validates the accuracy of this first-principles approach. The polarization-angular analysis reveals that extensions of the pores along the [001] direction are extremely important for Δn, which explains the qualitative different Δn observed in p^{+} and p^{++} *b*-PSi samples,[13] since in the former case there are pore branches along [001] direction. In contrast, for the p^{++} case, the pores are essentially aligned in the [100] and [010] directions; this causes Δn to always be positive, proportional to the porosity, and to decay with the wavelength. All these features are well reproduced in this first-principle calculation, confirming the fact that the pores are straight in the p^{++} doped *b*-PSi samples.

It is important to stress that porous silicon is a structurally complex system and the approach presented in this paper does emphasize the essential feature of *b*-PSi. Therefore, it is remarkable that this approach with no adjustable parameters is able to predict correctly the general behavior of optical properties of *b*-PSi by means of a small supercell and thus, a reduced computing effort. The results also show that all the studied *b*-PSi structures expand during the geometry optimization process, as observed in nonbirefringent PSi.[31] Finally, optical anisotropy measurements can be also employed to determine the local or average morphology of pores, as suggested in Ref. 32.

ACKNOWLEDGMENTS

This work has been partially financed by CONACyT Project No. 49291 and DGAPA-UNAM Project No. IN110305. The technical assistance of Silvia Frausto del Río and the critical reading of the manuscript by Roberto S. Capuano and Julia Tagüeña are fully appreciated.

[1] C. P. Poole and F. J. Owens, *Introduction to Nanotechnology* (Wiley, New York, 2003).
[2] Z. H. Lu, D. J. Lockwood, and J.-M. Baribeau, Nature (London) **378**, 258 (1995).
[3] P. Y. Yu and M. Cardona, *Fundamentals of Semiconductors* (Springer-Verlag, Berlin, 2001).
[4] L. T. Canham, Appl. Phys. Lett. **57**, 1046 (1990).
[5] L. Seals, J. L. Gole, L. A. Tse, and P. T. Hesketh, J. Appl. Phys. **91**, 2519 (2002).
[6] R. Nava, V. Agarwal, J. A. del Rio, and C. Wang, J. Non-Cryst. Solids **329**, 140 (2003).
[7] K. D. Hirschman, L. Tsybeskov, S. P. Duttagupta, and P. M. Fauchet, Nature (London) **384**, 338 (1996).
[8] S. Ben-Tabou de Leon, A. Sa'ar, R. Oren, M. E. Spira, and S. Yitzchaik, Appl. Phys. Lett. **84**, 4361 (2004).
[9] A. G. Cullis, L. T. Canham, and P. D. J. Calcott, J. Appl. Phys. **82**, 909 (1997).
[10] M. Christophersen, J. Carstensen, S. Rönnebeck, C. Jäger, W. Jäger, and H. Föll, J. Electrochem. Soc. **148**, E267 (2001).
[11] J. Diener, N. Künzner, D. Kovalev, E. Gross, V. Yu. Timoshenko, G. Polisski, and F. Koch, Appl. Phys. Lett. **78**, 3887 (2001).
[12] E. Gross, D. Kovalev, N. Künzner, V. Yu. Timoshenko, J. Diener, and F. Koch, J. Appl. Phys. **90**, 3529 (2001).
[13] N. Künzner, J. Diener, E. Gross, D. Kovalev, V. Yu. Timoshenko, and M. Fuji, Phys. Rev. B **71**, 195304 (2005).
[14] P. Hohenberg and W. Kohn, Phys. Rev. **136**, B864 (1964).
[15] R. G. Parr and W. Yang, *Density-Functional Theory of Atoms and Molecules* (Oxford University Press, New York, 1989).
[16] M. C. Payne, M. P. Teter, D. C. Allan, T. A. Arias, and J. D. Joannopoulos, Rev. Mod. Phys. **64**, 1045 (1992).
[17] M. S. Hybertsen and S. G. Louie, Phys. Rev. B **34**, 5390 (1986).
[18] R. Del Sole and R. Girlanda, Phys. Rev. B **48**, 11789 (1993).
[19] J. Harris and R. O. Jones, J. Phys. F: Met. Phys. **4**, 1170 (1974).
[20] M. D. Segall, P. J. D. Lindan, M. J. Probert, C. J. Pickard, P. J. Hasnip, S. J. Clark, and M. C. Payne, J. Phys.: Condens. Matter **14**, 2717 (2002).
[21] H. J. Monkhorst and J. D. Pack, Phys. Rev. B **13**, 5188 (1976).
[22] W. H. Press, B. P. Flannery, S. A. Teukolsky, and W. T. Vetterling, *Numerical Recipes* (Cambridge University Press, Cambridge, 1986).
[23] M. Cruz, M. R. Beltrán, C. Wang, J. Tagüeña-Martínez, and Y. G. Rubo, Phys. Rev. B **59**, 15381 (1999).
[24] R. Hull, *Properties of Crystalline Silicon*, Emis Series (INSPEC, London, 2000).
[25] V. Olevano, M. Palummo, G. Onida, and R. Del Sole, Phys. Rev. B **60**, 14224 (1999).
[26] J. Pastrnak and K. Vedam, Phys. Rev. B **3**, 2567 (1971).

[27]Y. Bonder and C. Wang, Phys. Status Solidi A **202**, 1552 (2005).
[28]O. Bisi, S. Ossicini, and L. Pavesi, Surf. Sci. Rep. **38**, 1 (2000).
[29]J. D. Jackson, *Classical Electrodynamics*, 3rd ed. (Wiley, New York, 1999), p. 334.
[30]H. A. Lorentz, *Collected Papers* (Martinus Nijhoff, The Hague, 1936).
[31]E. Vázquez, J. Tagüeña-Martínez, L. E. Sansores, and C. Wang, J. Appl. Phys. **91**, 3085 (2002).
[32]Y. Bonder and C. Wang, Mater. Res. Soc. Symp. Proc. **832**, F10.8 (2005).